The Astrophysical Journal, 580:305–316, 2002 November 20

MID-INFRARED IMAGING OF NGC 6334 I

James M. De Buizer,[1,2] James T. Radomski,[3] Robert K. Piña,[2,3] and Charles M. Telesco[3]
Received 2002 June 25; accepted 2002 July 23

ABSTRACT

We present high-resolution ($<0''.5$) mid-infrared Keck II images of individual sources in the central region of NGC 6334 I. We compare these images to images at a variety of other wavelengths from the near-infrared to centimeter radio continuum and speculate on the nature of the NGC 6334 I sources. We assert that the cometary shape of the ultracompact H II (UCHII) region here, NGC 6334F, is due to a champagne-like flow from a source on the edge of a molecular clump and not due to a bow shock caused by the supersonic motion of the UCHII region through the interstellar medium. The mid-infrared emission is concentrated into an arc of dust that defines the boundary between the UCHII region and the molecular clump. This dust arc contains a majority of the masers in the region. We discuss the nature of the four near-infrared sources associated with IRS I1 and suggest that one of the sources, IRS 1E, is responsible for the heating and ionizing of the UCHII region and the mid-infrared dust arc. Infrared source IRS I2, which has been thought to be a circumstellar disk associated with a linear distribution of methanol masers, is found not to be directly coincident with the masers and elongated at a much different position angle. IRS I3 is found to be a extended source of mid-infrared emission coming from a cluster of young dusty sources seen in the near-infrared.

Subject headings: H II regions — infrared: ISM — ISM: individual (NGC 6334I) — stars: formation

1. INTRODUCTION

NGC 6334 is a parsec-long train of rich molecular clouds and H II regions located at Galactic coordinates $l = 351°$, $b = 0°.7$. The complex lies at a distance of 1.74 kpc from the Sun (Neckel 1978), parallel to and located in the Carina-Sagittarius spiral arm. It is the site of possibly the largest number of recently formed OB stars observed in the Galaxy, which may have been triggered by the recent passage of a spiral density wave (Harvey & Gatley 1983).

NGC 6334 was first discovered in the far-infrared by Emerson, Jennings, & Moorwood (1973). Later observations in the far-infrared by McBreen et al. (1979) revealed six centers of emission. They were labeled by increasing southern declination using Roman numerals I–VI. Our observations were of NGC 6334 I, the northernmost far-infrared region of NGC 6334, and the site of a well-studied ultracompact H II (UCHII) region, NGC 6334F. Although heavily obscured at visual wavelengths, NGC 6334 I is the center of a wealth of activity in the infrared, millimeter, and radio, as well as the site of many molecular sources and masers. Over the decades, many authors have studied this region of NGC 6334, and each, it seems, used nomenclature of his or her own to describe it. NGC 6334 I is a large region that is identified with several significant sources summarized by Kraemer et al. (1999). We use the convention NGC 6334F from the radio continuum observations of Rodríguez, Cantó, & Moran (1982) to describe the UCHII region we observed in the mid-infrared. The H II region is clearly cometary shaped in the radio (Rodríguez et al. 1982; De Pree et al. 1995; Ellingsen, Norris, & McCulloch 1996), millimeter (Carral et al. 1997) and mid-infrared (De Buizer, Piña, & Telesco 2000; Persi et al. 1998), with its head pointing to the northwest and the tail running to the southeast. The peak of the UCHII region lies near the infrared source IRS I1 of Becklin & Neugebauer (1974), which has been presumed to be the ionizing source of the H II region. Harvey & Gatley (1983) also find another source $\sim6''$ to the northwest of IRS I1, designated IRS I2, and yet another $\sim18''$ to the east, designated IRS I3.

This region is very complex and is the site of a wide variety of activity. A near-infrared survey by Tapia, Persi, & Roth (1996) found an embedded young cluster of 93 sources associated with NGC 6334 I, all within a radius of $\sim80''$. This cluster, of which IRS I1, IRS I2, and IRS I3 are members, appears to contain only stars earlier than B3–B4, according to Tapia et al. (1996). In light of the complexity of the NGC 6334 I area, interpretation of data is not an easy task. In this paper we present high-resolution mid-infrared images of the sources within NGC 6334 I. In § 2 we discuss the observations of NGC 6334 I, and we explain the data reduction process in § 3. Interpretation of our data and a discussion of the phenomenology of each source is presented in § 4. Finally, in § 5 we present our conclusions.

2. INSTRUMENTATION AND OBSERVATIONS

Observations of NGC 6334 I were carried out in 1998 May and 1999 May on the Keck II 10 m telescope on Mauna Kea. Broadband N ($\lambda_0 = 10.46$ μm, $\Delta\lambda = 5.1$ μm) and IHW 18 (International Halley Watch; $\lambda_0 = 18.06$ μm, $\Delta\lambda = 1.7$ μm) imaging was performed using OSCIR, the University of Florida mid-infrared camera/spectrometer. OSCIR is equipped with a 128×128 pixel, silicon/arsenic-doped blocked impurity band (Si:As BIB) array that is optimized for 8–25 μm work.

At Keck II, OSCIR has a field of view of $8'' \times 8''$, for a scale of $0''.0616$ pixel^{-1}. Sky and telescopic radiative offsets were subtracted using a secondary chopping at 5 Hz and by nodding the telescope every 15 s. Frame times of 15 ms were

[1] Cerro Tololo Inter-American Observatory, National Optical Astronomy Observatory, Casilla 603, La Serena, Chile. CTIO is operated by AURA, Inc., under contract to the National Science Foundation.
[2] Visiting Astronomer, W. M. Keck Observatory.
[3] Department of Astronomy, University of Florida, Gainesville, FL 32611.

used for all observations. Images presented in this paper have total on-source integration times in both filters of 120 s for IRS I1, 480 s for IRS I2, and 240 s for IRS I3. The standard star α Boo was observed at roughly the same air mass ($\sim$1.7) as NGC 6334 I. It was used as a flux calibrator, with flux densities taken to be 683 Jy at N and 219 Jy at IHW 18. Point-spread function (PSF) stars were also imaged near the position of NGC 6334I, yielding a measured FWHM of $0\farcs33$ at N and $0\farcs41$ at IHW 18.

3. RESULTS AND DATA REDUCTION

We have observed NGC 6334I previously as part of a mid-infrared survey using the Cerro Tololo Inter-American Observatory (CTIO) 4 m telescope (De Buizer et al. 2000). The field of view at CTIO is large enough to encompass not only the UCHII region, but also the regions where IRS I2 and IRS I3 reside (Fig. 1). We were able to image the whole central region of NGC 6334 I at both 10 and 18 μm, although the extended emission from IRS I3 is slightly off-field in both filters. Because of the small field of view at Keck, we imaged the regions containing IRS I1, IRS I2, and IRS I3 individually (Fig. 1). Carral et al. (1997) detect an additional source just southeast of IRS I2 at 7 mm. Not only was it not detected in the J, H, and K images of Persi et al. (1996), we did not detect it in our images from CTIO at either 10 or 18 μm (De Buizer et al. 2000). Because of time constraints, we did not obtain follow-up images centered on this 7 mm source at Keck.

3.1. *Flux Calibration*

Because of the large bandwidth of the filters, the observed fluxes must be color-corrected to account for the intrinsic source spectrum, the filter transmission, and the atmospheric transmission. For the calibration stars, the spectra were assumed to be a blackbody at the effective stellar temperature. Color-corrected monochromatic flux densities, dust color temperatures, and optical depth values were obtained in a self-consistent manner by iteratively performing a numerical integration on the product of the Planck function, emissivity function (given by $1e^{-\tau_\lambda}$, where τ_λ is given by the extinction law of Mathis 1990), filter transmission, solid angle subtended by the source, and model atmospheric transmission through the filter bandpass. A detailed treatment of this color-correction method is given in De Buizer (2000). As is often the case with mid-infrared observations, the calibration factor (ratio of accepted flux in janskys to analog-to-digital converter units per second per pixel) derived from the standard star observations changed throughout the course of the night as a result of changes in atmospheric conditions, but there was little correlation with air mass. Therefore, air mass corrections were not made to the observations. We can, however, estimate the absolute photometric accuracy (i.e., the mean calibration value of the standard star observations throughout the night divided by the standard deviation) associated with the tabulated color-corrected flux densities in Table 1 to be 6.8% at 10 μm and 9.7% at 18 μm.

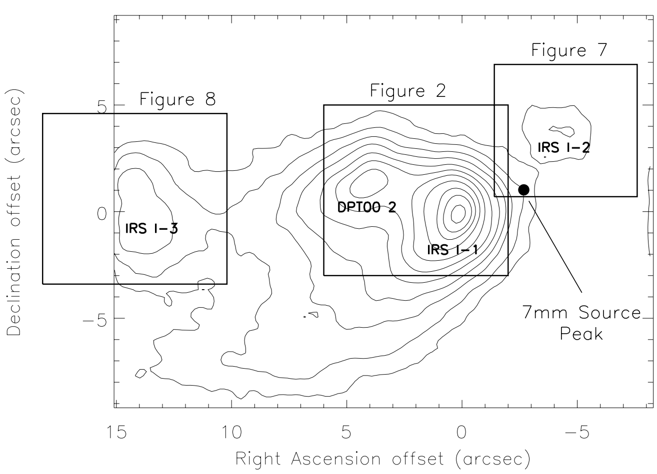

FIG. 1.—Central region of NGC 6334I at 18 μm. This image was taken at the CTIO 4 m by De Buizer et al. (2000) at a resolution of $\sim1''$. The individual fields that were imaged at Keck are shown as boxes. At the center of this image is NGC 6334F, a cometary UCHII region. It can be seen as two separate sources in the mid-infrared, IRS I1 and DPT00 2. Also labeled is the location of the 7 mm source seen by Carral et al. (1997). This source was not detected in our mid-infrared images. The coordinates of the origin are R.A. (J2000.0) = $17^{\rm h}20^{\rm m}53\fs44$ and decl. (J2000.0) = $-35°47'02\farcs2$.

3.2. *Temperature and Optical Depth Maps*

One advantage of acquiring images at two wavelengths at Keck II is that we were able to construct dust color temperature (T) and emission optical depth (τ) maps for each source. This was accomplished by first convolving the 10 μm source images with the 18 μm image of a PSF star and the 18 μm source images with the 10 μm PSF image. This step is important because artificial structures in the temperature and optical depth maps can result from failure in having both images at the same resolution. This convolution process gives an effective resolution of the temperature and optical depth maps of $0\farcs53$. The relative alignment of the two images is also crucial to the values derived for temperature and optical depth. We employed an automated registration algorithm based on minimizing the sum of the squared residuals of the image difference as a function of the relative offsets. This algorithm generates a χ^2 surface at integral x and y pixel offsets. The χ^2 surface may then be interpolated to determine the location of the minimum to a hundredth of a pixel. Best-fit alignments for the image sets were found in this way for all sources.

Once an image set was spatially registered, the 10 and 18 μm flux densities for each pixel were used to iteratively solve for emission optical depth (τ) at 10 μm and dust color temperature under the assumption of blackbody emission. For these calculations we used the relationship $\tau_{10\,\mu\rm m} = \tau_{18\,\mu\rm m}/1.69$ from the extinction law of Mathis (1990). A cutoff was applied to both the 10 and 18 μm flux density maps at 3 σ above the background sky value. Temperature and optical depth values were calculated only for those areas that were above this cutoff at both wavelengths. The relative alignments of the 18 and 10 μm source images were then shifted by 4 pixels ($0\farcs25$) in various directions. It is unlikely that our registration of the images is off by such a large amount; however, this allows a test of the robustness of the results concluded from the temperature and optical depth maps. It was found that these shifts significantly changed the peak temperature and optical depth values ($\pm$25%); however, these shifts created only slight changes ($<0\farcs3$) in the peak locations and overall morphologies. Therefore, while there may be uncertainty in the absolute values for these temperatures and optical depths, the maps are quite

TABLE 1
PROPERTIES OF SOURCES IN NGC 6444 I

Source	10 μm Flux Density[a] (Jy)	18 μm Flux Density[a] (Jy)	Offset[b] ($\Delta\alpha$, $\Delta\delta$) (arcsec)	Right Ascension[b] (J2000.0)	Declination[b] (J2000.0)	Luminosity[c] ($L_\odot$)	ZAMS Spectral Type[c]
IRS-I-1	78.63 ± 5.42	222.70 ± 21.60	(0, 0)	17 20 53.44	−35 47 02.2	3285	B2
IRS-I-2[d]	0.13 ± 0.01	3.41 ± 0.33	(−4.8, +3.9)	17 20 53.04	−35 46 58.3	67	B9
IRS-I- 3 (all)....	2.22 ± 0.15	22.96 ± 2.23	(+14.1, −0.4)	17 20 54.60	−35 47 02.6	326	B7
North lobe...	1.09 ± 0.07	8.57 ± 0.83	...	...	...	117	B9
South lobe ...	1.24 ± 0.08	12.87 ± 1.25	...	...	...	183	B8
DPT00 2	11.37 ± 0.77	68.65 ± 6.66	(+4.0, +1.6)	17 20 53.77	−35 47 00.6	919	B4

NOTE.—Units of right ascension are hours, minutes, and seconds, and units of declination are degrees, arcminutes, and arcseconds.

[a] Color-corrected flux densities. The quoted errors in the measurements are the absolute photometric accuracy for the night (the dominant source of error), which was calculated to be 6.8% at 10 μm and 9.7% at 18 μm. All extended emission in the frames is included for all sources and may lead to the small differences between the values quoted here and that of De Buizer et al. 2000.

[b] Refer to the text and Figs. 7 and 8 for locations of these coordinates for the extended sources IRS I2 and IRS I3.

[c] Luminosities and spectral types are given for all objects for the sake of completeness. Some sources may not actually have stellar cores or may be heated by more than one star (see text).

[d] Flux densities for IRS I2 are much different than those quoted in De Buizer et al. 2000. This is most likely because the CTIO 4 m images yielded very low signal-to-noise ratio for IRS I2.

useful in demonstrating the spatial trends of these properties for these sources. The lower spatial scale color temperature and optical depth maps of Kraemer et al. (1999) look very similar to our maps, indicating that the structures in these maps are real.

3.3. *Astrometry*

Because of time constraints, careful astrometry was not performed. Therefore, accurate astrometry of the images needed to be performed by registering the mid-infrared images with other wavelength data. In the case of De Buizer et al. (2000), the 5.0 cm radio continuum map of Caswell (1997) was registered with the mid-infrared images by aligning the radio and mid-infrared morphologies and peaks. Even with the higher spatial resolution images from Keck, it was found that the astrometry used in De Buizer et al. (2000) does indeed show the best morphological coincidences between the mid-infrared images of NGC 6334F and images at other wavelengths. We cannot be completely sure that this is the correct astrometry because the morphologies may be wavelength-dependent. However, this registration does show surprisingly good morphological coincidences throughout a broad range of wavelengths (6.2, 5.0, 3.5, 2.0, 1.3, and 2.2 μm), as we will discuss in more detail in § 4.1. We therefore feel that the absolute astrometry of our mid-infrared sources is good to $\leq 0\farcs5$.

3.4. *Luminosity and Spectral Type*

Estimates of zero-age main-sequence (ZAMS) stellar luminosities were made for each of the objects based upon their mid-infrared color-corrected fluxes. These are presented in Table 1. These values are based on the simplified assumption that all of the luminosity seen at the mid-infrared wavelengths is dust-reprocessed stellar radiation and so is indicative of the true bolometric luminosity of the stellar source itself. These mid-infrared luminosity estimates were computed by integrating the Planck function from 1 to 600 μm at the derived dust color temperature and optical depth for each source. This calculation employs the above emissivity function and assumes emission into 4π sr. Using the tables of Doyon (1990), which are based on the stellar atmospheric models of Kurucz (1979), we then found the ZAMS spectral types associated with those mid-infrared derived luminosities.

The main problems with this method of deriving estimates to the bolometric flux are (1) if the dust is anisotropically distributed around the source, the derived luminosity would depend on this dust distribution because some of the stellar flux will escape unprocessed through the unobstructed regions; (2) heavy obscuration could lead to nonnegligible reprocessing by dust of the mid-infrared photons into far-infrared photons; and (3) dust is in competition with gas for the short wavelength photons, which ionize the gas and produce UCH II regions. All of these processes would lead to underestimates of the bolometric luminosities from mid-infrared fluxes; however, it is hard to quantify exactly how each contribute. For these reasons we believe that the derived bolometric luminosities represent good lowers limit to the true bolometric luminosities.

As we will discuss later in the paper, some of these sources are believed not to be centrally heated. Therefore, the derived ZAMS spectral types in reality will not apply, and the luminosity given in Table 1 is a better indication of the infrared luminosity of the source, rather than the bolometric luminosity.

4. DISCUSSION OF INDIVIDUAL SOURCES

4.1. *NGC 6334F* (*IRS I1 and DPT00 2*)

Mid-infrared observations of the UCHII region NGC 6334F have revealed that it is composed of two sources (De Buizer et al. 2000; Kraemer et al. 1999). Our brightest mid-infrared peak (Fig. 2) is apparently the same as the peak of the cometary UCHII region seen in the radio maps of NGC 6334F. Another mid-infrared source lies 4″ northeast of the mid-infrared peak and is elongated in its thermal dust distribution. This source has been designated G351.42+0.64:DPT00 2 by De Buizer et al. (2000) and is also referred to as NGC 6334:MFSW I:KDJ 4 by Kraemer et al. (1999). Throughout this paper we will refer to this source as DPT00 2 (Fig. 1).

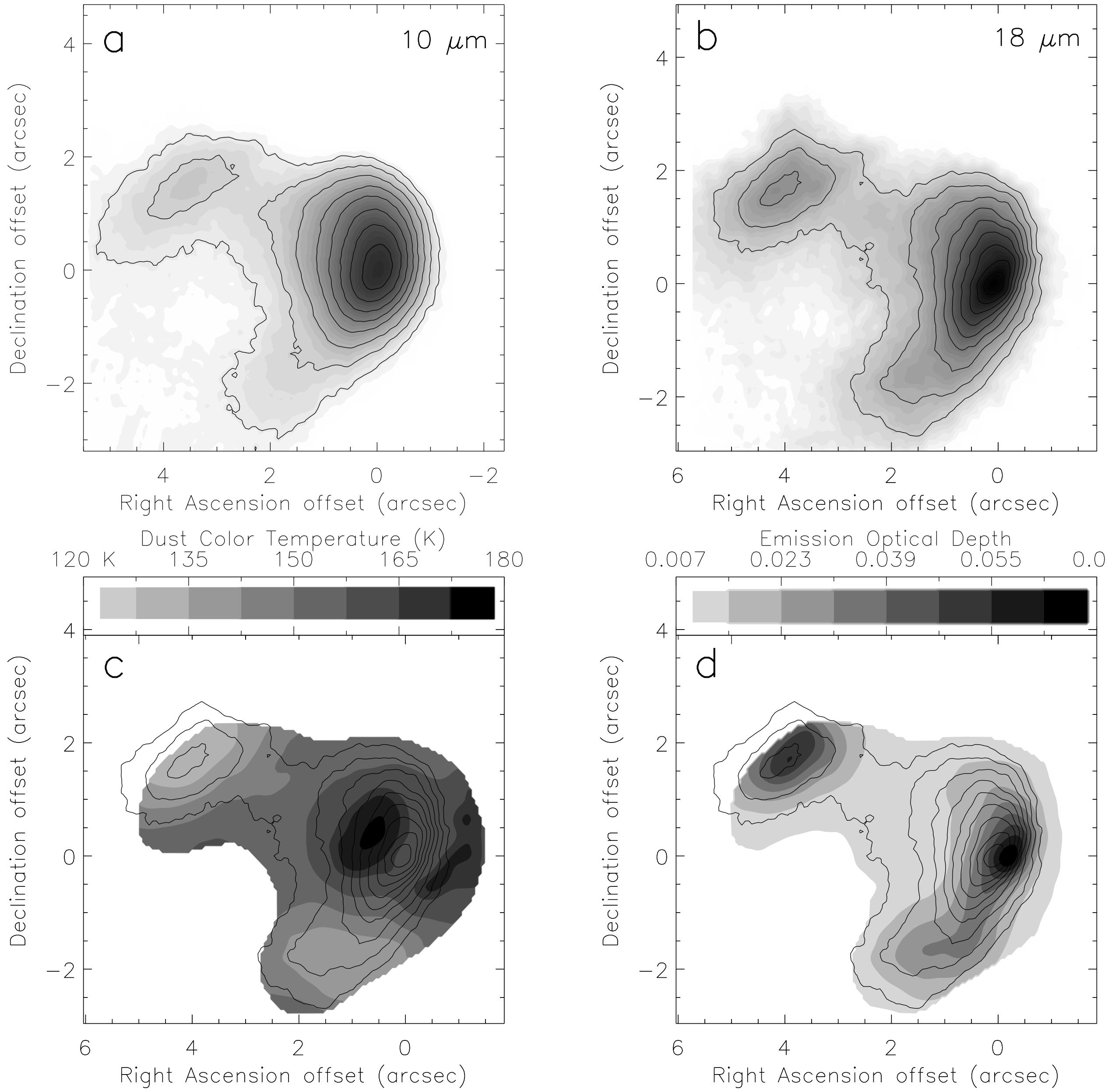

FIG. 2.—Keck data for NGC 6334F. (*a*) and (*b*) show the OSCIR images in gray scale at 10 and 18 μm, respectively, convolved with a Gaussian kernel of FWHM 2 pixels. Contours are added for emphasis. In (*a*) contour levels are 3, 4, 5, 6, 9, 12, 16, and 22 Jy arcsec^{-2}. In (*b*) contour levels are 6.5, 10, 15, 20, 30, 40, 50, 60, and 80 Jy arcsec^{-2}. (*c*) shows the color temperature map of the region, and (*d*) shows the emission optical depth map, both with the 18 μm contours overlaid. The origin in each panel is the same as in Fig. 1.

4.1.1. *Temperature and Optical Depth Maps*

In Figure 2*d* one sees that the 18 μm contours of IRS I1 delineate the optical depth contours (*gray scale*) fairly well. Looking at an overlay of the dust color temperature and the 18 μm map (Fig. 2*c*), the temperature peak is offset from the 18 μm peak. Both of these observations indicate that the mid-infrared emission is bright there simply because it is optically thin in the mid-infrared and we are seeing through more material in the line of sight. This is a ridge of material that could have be swept-up dust from the expanding shock front of the UCHII region. This leads to the conclusion that the mid-infrared peak may not be delineating the location of the exciting stellar source for the UCHII region.

4.1.2. *Radio Continuum*

The UCHII region of NGC 6334F has been extensively observed at radio wavelengths. Because of similar spatial resolution (FWHM $\sim 0\farcs5$) and morphology, we used the 3.5 cm radio maps of Carral et al. (2002) to achieve accurate astrometry of our mid-infrared maps (Fig. 3*a*). Using this astrometry, we also checked the mid-infrared morphology against other radio contour maps at similar resolution: the 5 cm (FWHM $\sim 2''$) of Caswell (1997), the 3.6 cm (FWHM $\sim 1\farcs2$) of Ellingsen, Norris, & McCulloch (1996), and the 2.0 cm map (FWHM $\sim 1\farcs0$) of De Pree et al. (1995) (Fig. 3*b*). In all cases, the radio contours corresponded closely to those of the mid-infrared around the UCHII

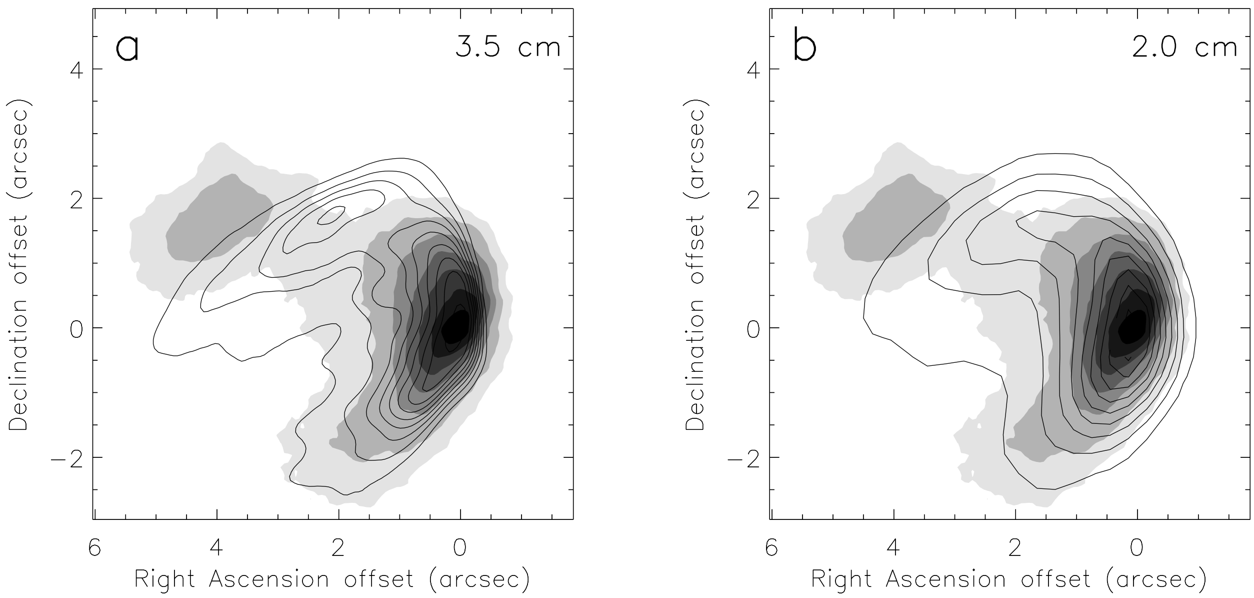

FIG. 3.—Comparisons of the 18 μm images (*filled contours*) with radio continuum images (*contours*) demonstrate that the contours of the radio continuum and mid-infrared are correlated for IRS I1. (*a*) The 3.5 cm radio continuum images of Carral et al. (2002) registered with respect to the mid-infrared image. By registering the mid-infrared images with respect to the radio continuum images, the mid-infrared absolute astrometry was determined. (*b*) The registration between the 2.0 cm maps of De Pree et al. (1996) and the mid-infrared. The origin in both panels is the same as in Fig. 1.

region peak, adding confidence to the idea that the radio and mid-infrared emission are coming from the same location. Comparing the radio maps with the mid-infrared images shows that radio emission comes not only from the location of the peak of the UCHII region, but from DPT00 2 as well. The radio continuum emission seems to trace the southern edge of DPT00 2 where it faces the peak of the UCHII region, indicating that it may be externally ionized. The color temperature maps are consistent with this scenario. The southern edge of DPT00 2 is also the hottest part of the source and therefore may not be internally heated (Fig. 2*c*).

4.1.3. *Comparisons to the Observations of Harvey & Gatley* (*1983*)

The peak in the UCHII region at 18 μm apparently corresponds to the IRS I1 peak of Harvey & Gatley (1983). Overlays between our 18 μm mid-infrared maps and the 20 μm mid-infrared maps of Harvey & Gatley (1983) show similar morphology with two peaks with the same separations as IRS I1 and IRS I2 (Fig. 4*a*). The 20 μm maps of Harvey & Gatley (1983) show extension in the direction of DPT00 2 but do not resolve the source. Using the astrometry above, we find that the absolute coordinates of the 20 μm peaks of IRS I1 and IRS I2 from Harvey & Gatley (1983) are both in error by approximately $1\rlap{.}''5$ in the southern direction. This is entirely plausible, given that these observations were performed by scanning the area with a photometer with a $4''$ beam, although the quoted positional accuracy is $1''$. Assuming that our astrometry is correct and using the coordinates of the peak of the radio continuum from Carral et al. (2002), the mid-infrared peak of IRS I1 is at R.A. (J2000.0) $= 17^{\rm h}20^{\rm m}53\rlap{.}^{\rm s}44$, decl. (J2000.0) $= -35°47'02\rlap{.}''16$. This changes the mid-infrared coordinates for the other sources as well. These new coordinates are given in Table 1.

4.1.4. *Ammonia Distribution*

Ammonia observations by Kraemer & Jackson (1995) show the UCHII region to be bounded by ammonia (3, 3) emission to the west. This emission is a dense gas indicator, as is CS $7 \rightarrow 6$, which also peaks west of the UCHII region (Kraemer et al. 1999). It appears therefore that the star responsible for ionizing the UCHII region exists on the edge of this density enhancement, and this gradient in the surrounding medium is what has led to the shape of the UCHII region. These observations seem to indicate that the cometary appearance is due to a champagne-like flow rather than a bow shock caused by supersonic motion through the interstellar medium.

Figure 7 of Kraemer et al. (1999) shows an overlay of their mid-infrared and ammonia observations by registering them using the coordinates of Harvey & Gatley (1983), which we believe to be in error. We present in Figure 4*b* the correctly registered integrated ammonia map of Kraemer et al. (1999) and our mid-infrared map of the region. Because the radio continuum and ammonia maps were taken at the same time, they have extremely accurate relative astrometry. We overplotted the integrated ammonia in Figure 4*b* by first registering the radio continuum peak of Kraemer et al. (1999) with our mid-infrared peak for IRS I1. The integrated ammonia map presented in Figure 4*b* is mostly ammonia emission but also contains ammonia seen in absorption. The weakest contour of ammonia in the integrated map appears to wrap around the mid-infrared peak in Figure 4*b*. This ammonia component is associated with the mid-infrared (and radio continuum) peak and is actually seen in absorption by Kraemer & Jackson (1995). The rest of the integrated map shows ammonia emission, bounded by IRS I1 to the east and IRS I2, lies just to the west of the secondary peak. The ammonia emission follows along the eastern edge of the UCHII region, extending to the south.

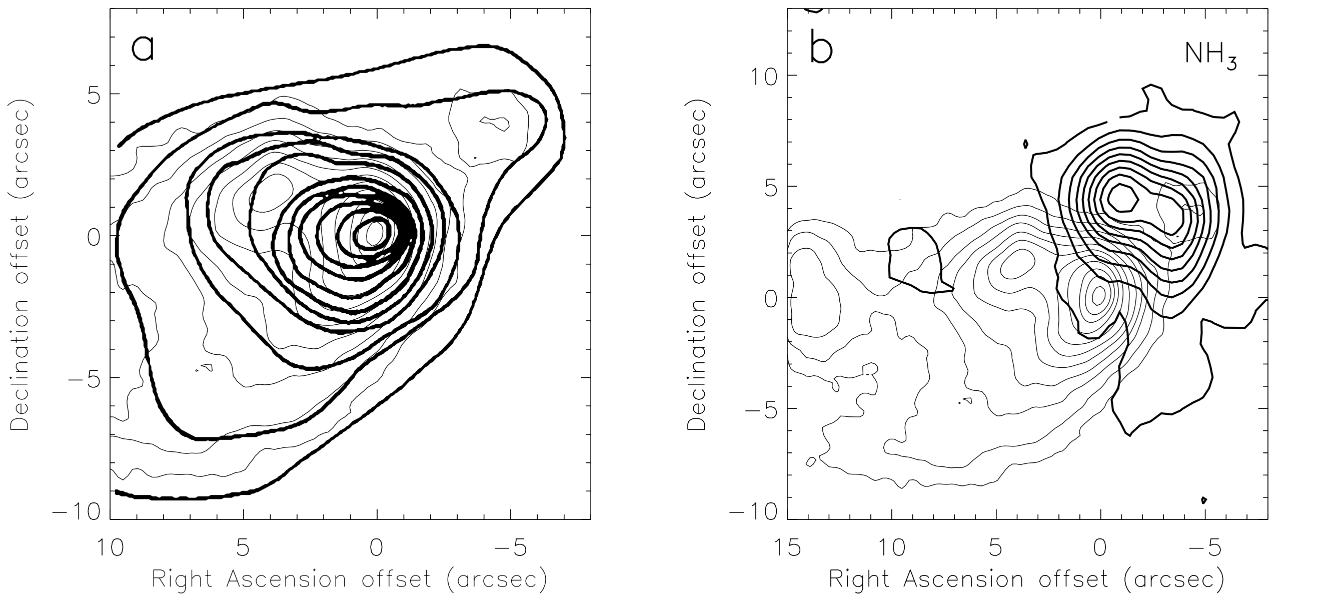

FIG. 4.—Comparisons of the 18 μm emission from NGC 6334 I with other large-scale emission. (*a*) The 20 μm (*thick*) contours of Harvey & Gatley (1983) compared to the 18 μm (*thin*) contours from De Buizer et al. (2000). A very good match is found, leading us to a revision in the mid-infrared coordinates of Harvey & Gatley (1983). (*b*) The integrated ammonia map (*thick contours*) of Kraemer et al. (1999) registered with respect to the mid-infrared images from De Buizer et al. (2000, *thin contours*) using the new mid-infrared coordinates. The ammonia appears to bound the UCHII region on to the west and may be responsible for the champagne-like flow manifesting itself as the cometary shaped UCHII region. The origin in both panels is the same as in Fig. 1.

4.1.5. *Masers*

The maser emission in this region is concentrated near IRS I1 (Fig. 5). This area is marked by several molecular maser species: methanol (Ellingsen et al. 1996), water (Forster & Caswell 1989), and hydroxyl (Gaume & Mutel 1987). A majority of the masers seem to be on the sharp western edge of the UCHII region, which is bounded by the ammonia emission (Figs. 5*a* and 5*b*). This density enhanced side of the UCHII region will also be a location where the expansion of the ionized material will first impact as a shock front. The density and energetics of such a region would be suitable for creating and sustaining maser emission. If this is the case, the masers that exist on this sharp boundary may be shock-induced.

There is a long string of water masers that are offset to the north of the mid-infrared emission from the IRS I1. Strings of water masers can be interpreted as coming from and delineating outflow (e.g., Claussen et al. 1997). However, water masers are also known to exist coincident with "hot cores," as seen from their molecular emission (Cesaroni et al. 1994). Observations of G9.62−0.19 (Hofner & Churchwell 1996) show a string of water masers emanating radially from a UCHII region center. However, the ammonia obser-

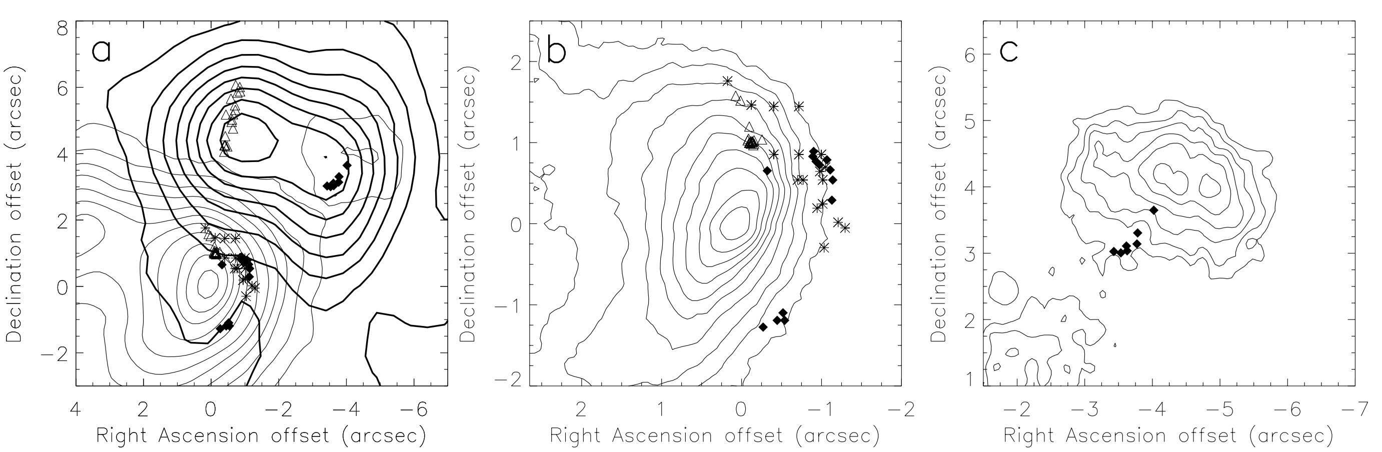

FIG. 5.—Water (*triangles*), hydroxyl (*stars*), and methanol (*filled diamonds*) masers in the NGC 6334 I region. (*a*) shows that a majority of the masers are associated with the sharp boundary between the 18 μm emission (*thin contours*) of IRS I1 and the ammonia emission (*thick contours*). This 18 μm image is from the CTIO 4 m telescope (De Buizer et al. 2000). A string of water masers may be associated with the brightest peak of the ammonia distribution, and a string of methanol masers may be associated with the secondary peak. (*b*) zooms in closer to IRS I1 to show that the masers are all excited along the sharp western edge of the source. (*c*) shows that the methanol masers that were thought to be associated with IRS I2 are not coincident with the mid-infrared source peak. The origin in each panel is the same as in Fig. 1.

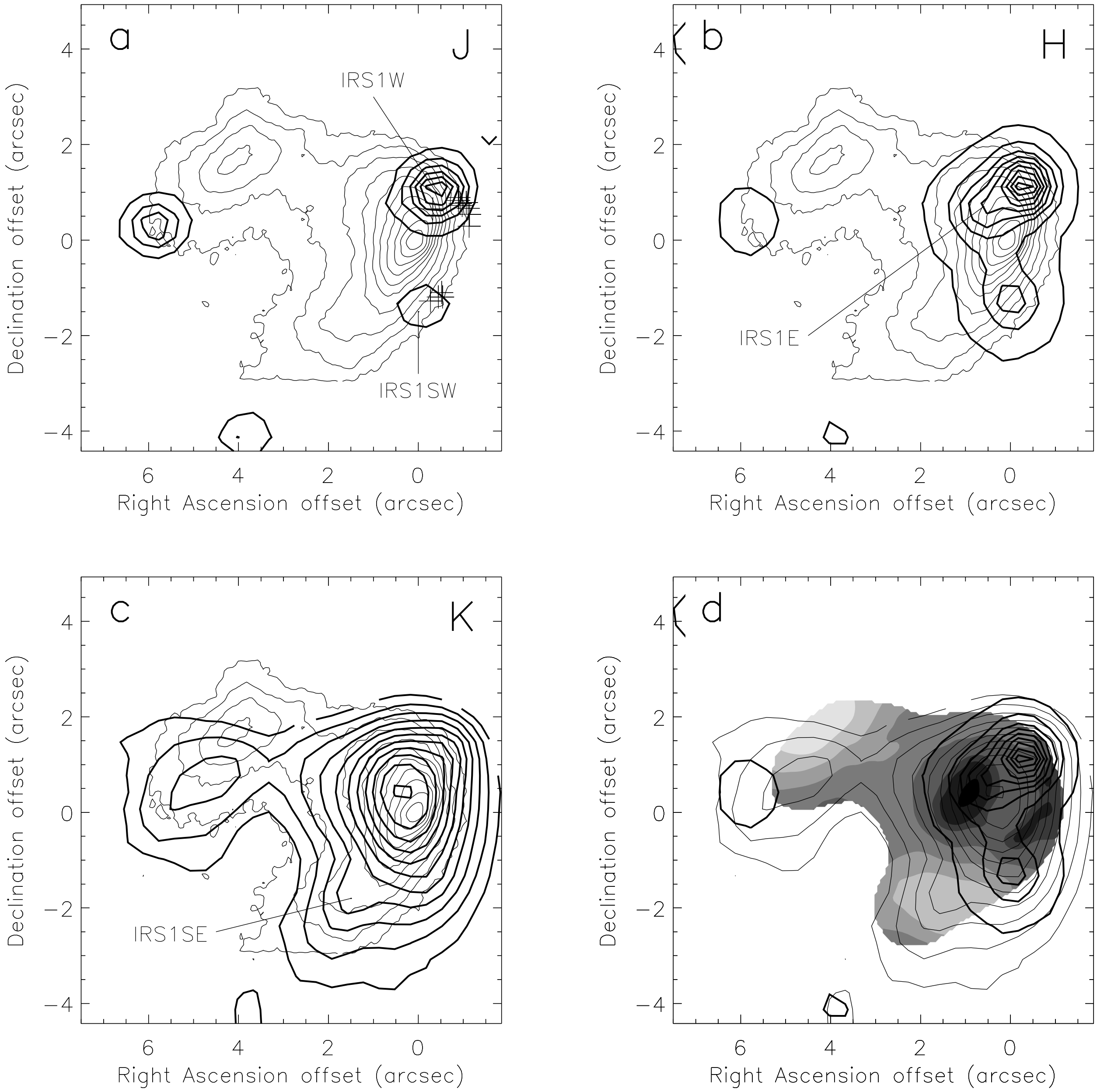

FIG. 6.—Near-infrared sources in the region near IRS I1 from Persi et al. (1996). (*a*), (*b*), and (*c*) show the near-infrared (*thick contours*) *J*, *H*, and *K* images, respectively, overplotting the 18 μm Keck (*thin*) contours. Labels are the names of the near-infrared sources given by Persi et al. (1996). The methanol masers are plotted in (*a*) as crosses. They appear to be associated with two near-infrared sources. (*d*) The color temperature map (*filled contours*) overlaid with the *K* emission (*thin contours*) and *H* emission (*thick contours*). The origin in each panel is the same as in Fig. 1.

vations of Cesaroni et al. (1994) show a peak at the same position as the water masers, and it has been proposed that these water masers are delineating the location of a hot core. Likewise, given the corrected astrometry set forth in this paper, the primary ammonia peak north of IRS I1 is coincident with the water maser string. It is plausible that these water masers are delineating the site of a hot core.

There is also a group of methanol masers that are offset northwest of IRS I1, that are thought to be associated with IRS I2 (Fig. 5*c*). Our astrometry shows that they are not exactly coincident with this mid-infrared source, and are close to the secondary ammonia peak (Fig. 5*a*). These methanol masers may be delineating a second hot core in the ammonia. Both of these maser strings may delineate the location of hot cores that are too cool and/or embedded to see in the thermal infrared.

4.1.6. *Mid-Infrared versus Near Infrared Sources*

Persi et al. (1996) observed this area in the near-infrared bands *J* (1.25 μm), *H* (1.65 μm), and *K* (2.2 μm) at a resolution of 0".9. These observations revealed four sources within 3" of the IRS I1 peak. The near-infrared sources are labeled IRS 1E, IRS 1W, IRS 1 SE, and IRS 1SW (Fig. 6). These sources are highly reddened and therefore believed not to be foreground stars. Persi et al. (1996) claims that the IRS 1E source is coincident with the 30 μm peak of Harvey & Gatley (1983). Overlaying the *K* image with our mid-infrared images shows good morphological coincidences with both IRS I1 and IRS I3 (see § 4.3), leading us to believe the relative astrometry between the near-infrared and mid-infrared to be better than 0."5. This alignment places IRS 1E peak approximately 1."8 from the 30 μm peak and 0."7 from our 18 μm peak.

Overlaying the *K*-band image with the color temperature map generated from our mid-infrared images we see a very important coincidence that once again leads us to believe our astrometry is correct (Fig. 6*d*). The color temperature is peaked near the location of a near-infrared source (IRS 1E). Also, there is a near-infrared source seen at *J* and *H*, and extended at *K*, coincident with the southeastern portion of DPT00 2 (Fig. 6*c*). We see in the temperature map in Figure 6*d* that the hottest parts of DPT00 2 are on the side facing the UCHII region. Since this region is hotter, it should be more readily seen in the near-infrared. These coincidences of the hotter regions to near-infrared emission seem to confirm our relative astrometry. The coincidence of IRS 1E to the peak in the color temperature map also leads us to speculate that the near-infrared source IRS 1E may be responsible for the central heating and ionizing of the UCHII region.

The nature of IRS 1W and IRS 1SW can also be speculated from the color temperature and optical depth maps. By looking at the near-infrared images of Persi et al. (1996) in Figure 6, we see that as one views this region at shorter and shorter wavelengths, the near-emission comes only from the sources within the mid-infrared arc of emission from IRS I1. Since the optical depth is largest at the mid-infrared peak, this is where there is a higher concentration of cooler material. At *J* and *H*, IRS 1W and IRS 1SW lie just north and just south of the mid-infrared peak (Figs. 6*a* and 6*b*). The near-infrared emission is coming from areas where thermal dust emission is located, but not at its densest and brightest parts. Furthermore, both of these sources are not temperature peaks in the color temperature map (Fig. 6*d*). If IRS 1W and IRS 1SW are not hot, there must be an alternate reason why they are visible in the near-infrared.

One scenario is that IRS 1W and IRS 1SW are visible in the near-infrared because of shock-excited emission (De Buizer 2002). These sources are most prominent at *J* and *H*, and both of these filter bandpasses encompass many lines of [Fe II]. These spectral lines are shock indicators (McKee, Chernoff, & Hollenbach 1984), two of the strongest being the lines at 1.26 and 1.64 μm (roughly the central wavelengths of the *J* and *H* filters). Bloomer et al. (1998) observed a diffuse UCHII region like NGC 6334F and find that the thermal dust emission and narrow line [Fe II] images are well matched spatially. As discussed above, the shape of the UCHII region and the presence of masers on the sharp western boundary imply that the masers may be shock-excited. In this same location there is a density enhancement of dust, as seen in the mid-infrared, which may be swept-up material from an expanding shock front rather than circumstellar in origin. IRS 1W is located on this dust ridge, is coincident with the majority of the masers here, and is most prominent in the *J* and *H* bands, which contain several lines that are shock indicators. For all of these reasons, it seems plausible that IRS 1W and IRS 1SW are not stellar sources themselves, but instead may be areas of shock excited emission. The final proof of such a hypothesis would be to obtain near-infrared spectra of these sources.

However, inconsistent this scenario is the near-infrared H_2 observation shown in the article by Persi et al. (1996), which does not seem to show any shock-excited H_2 emission at these locations. Greenhouse et al. (1991) finds that H_2 emission (a more widely used shock indicator) and [Fe II] are well correlated in their emission. Therefore, an alternative scenario could be that IRS 1W and IRS 1SW are simply areas of reflected emission from the less-extinguished parts of IRS I1.

As for the near-infrared source IRS 1SE, we see no mid-infrared source or peak at this location, but it is an area of diffuse mid-infrared emission. It seems that IRS 1SE is not a stellar source either and that the near-infrared emission may likely be coming from reflected or scattered photons off of the tail of the UCHII region.

4.2. *IRS I2*

The Keck images of IRS I2 reveal it to be an elongated and low-surface brightness source. The source has relatively low signal-to-noise ratio (peak pixel $S/N \sim 7$), but smoothing (3 pixel Gaussian) shows three peaks in the thermal emission along the direction of elongation (Fig. 7). The central and western peaks are comparable in brightness; however, the eastern source is fainter, especially at 18 μm. Because the western peak can be clearly seen at both 10 an 18 μm, we chose this location as the reference position for IRS I2 in Figure 7, and give the coordinates for this location in Table 1. Overlays of the NGC 6334I region from Harvey & Gatley (1983) and our 18 μm data show a good match in the peak locations, confirming that the source seen at Keck is indeed IRS I2 (Fig. 4*a*).

The source elongation in the mid-infrared is at a position angle of $\sim 65°$. The methanol masers near this source (Ellingsen et al. 1996) lie at an angle of approximately $-35°$, almost perpendicular to the thermal dust elongation (Fig. 5*c*). However, the masers are not coincident with IRS I2. The measured distance from the center of the maser distribution to the center of brightness in the 18 μm emission from IRS I2 is 1."25. Again, these masers lie close to the secondary peak in the thermal ammonia emission and may be delineating the sight of a second hot core or embedded protostar instead of being associated directly with the IRS I2.

Looking to the color temperature maps of this source show that the hottest part of the source is the eastern peak (Fig. 7*c*). By overlaying the optical depth maps with the 18 μm contours, one can see that the optical depth distribution for the central and western sources trace the 18 μm contours well (Fig. 7*d*). This implies that these two sources are bright merely because we are seeing through more optically thin mid-infrared emitting material. As in the case for IRS I1, it may be likely that the stellar heating source does not lie at the mid-infrared peak and that the temperature peak may be the location of the stellar source. However, there are two reasons that this argument may not be applicable in this instance. First, unlike IRS I1, we cannot be sure that the temperature peak is the location of the stellar source because there is no near-infrared component at this location (Persi et al. 1996). If it is hotter we would expect the energy distribution to rise toward the near-infrared, in the absence of significant extinction. This leads to a second point, which is that the temperature "peak" in this case is only 12 K hotter than the coolest parts of the source. This is unlike

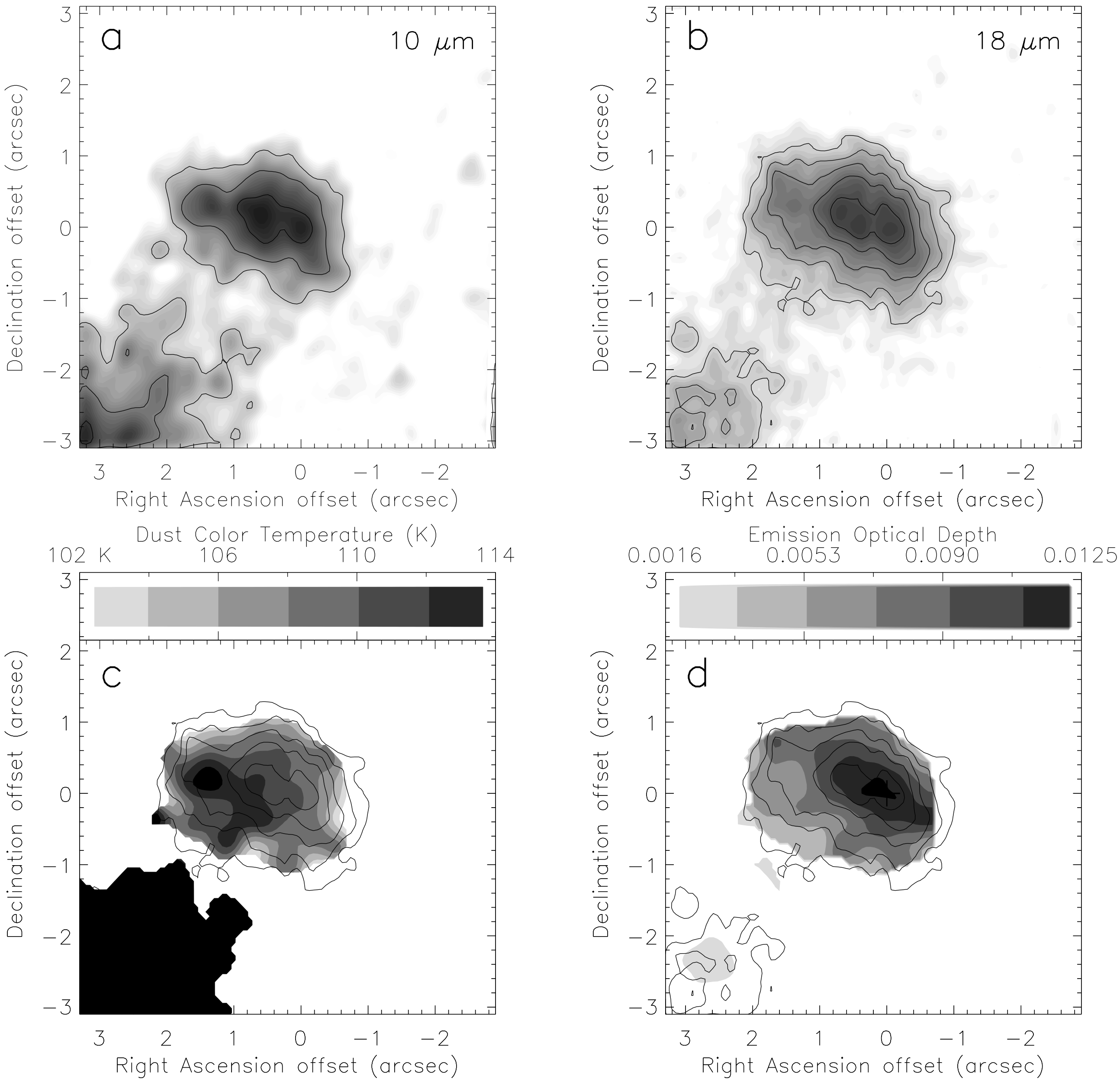

Fig. 7.—Keck data for IRS I2. (*a*) and (*b*) show the OSCIR images in gray scale at 10 and 18 μm, respectively, convolved with a Gaussian kernel of FWHM 3 pixels. Contours are added for emphasis. In (*a*) contour levels are 15, 40, and 60 mJy arcsec^{-2}. In (*b*) contour levels are 200, 400, 600, 800, and 1000 mJy arcsec^{-2}; (*c*) shows the color temperature map of the region and (*d*) shows the emission optical depth map, both with the 18 μm contours overlaid. The origin in each panel is R.A. (J2000.0) $= 17^{\rm h}20^{\rm m}53\overset{\rm s}{.}04$ and decl. (J2000.0) $= -35°46'58\overset{\prime\prime}{.}3$.

IRS I1, where the temperature peak is definitive because it is twice as hot ($\Delta T = 60$ K) as the coolest areas mapped. Given the fact that the source is relatively flat in both mid-infrared flux and color temperature, IRS I2 may not be internally heated. Because the temperature map shows this source to be warmest on the side facing the ammonia peak, if there is an embedded stellar or protostellar source at this location, it may be responsible for this slight heating of IRS I2. This side of the molecular core would have to have less extinction than the side facing the earth, allowing heating of IRS I2 without a direct view of the heating source from the earth.

There is mid-infrared emission in the southeast corner of the images of IRS I2 from Keck (Fig. 7*a*). This emission is located approximately where we would expect the 7 mm source of Carral et al. (1997) to be located. However, the emission is diffuse and cutoff by the edge of the array. It is most likely just extended emission from IRS I1. The most recent high-sensitivity study of this source was performed by Carral et al. (2002) and does not confirm the detection of this source at 7 mm. They claim that the source seen in their previous 7 mm study may have been an artifact of the data reduction and the limited (u, v) coverage of the observations.

4.3. *IRS I3*

This source has low surface brightness and is hourglass-shaped in the mid-infrared; however, the northern lobe of

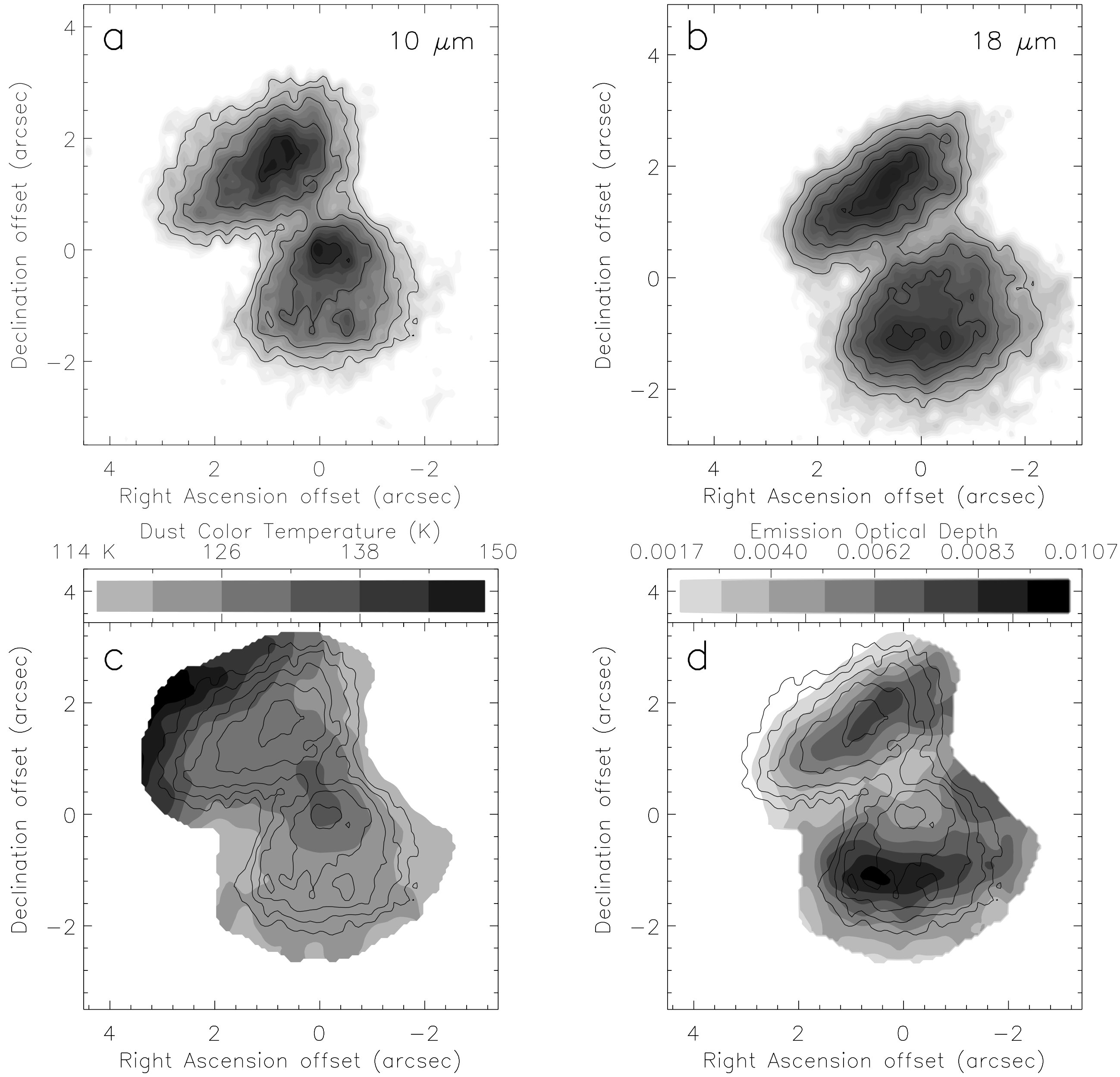

FIG. 8.—Keck data for IRS I3. (*a*) and (*b*) show the OSCIR images in gray scale at 10 and 18 μm, respectively, convolved with a Gaussian kernel of FWHM 3 pixels. Contours are added for emphasis. In (*a*) contour levels are 65, 85, 110, 150, and 200 mJy arcsec^{-2}. In (*b*) contour levels are 600, 800, 1000, 1250, and 1600 mJy arcsec^{-2}; (*c*) shows the color temperature map of the region; and (*d*) shows the emission optical depth map, both with the 18 μm contours overlaid. The origin in each panel is R.A. (J2000.0) $= 17^{\rm h}20^{\rm m}54\overset{\rm s}{.}60$ and decl. (J2000.0) $= -35°47'02\overset{''}{.}6$. The apparent offset between (*a*) and (*b*) is not real, but simply a change in the position of the origin in the panels.

the source is more extended in the northern direction at 10 than at 18 μm (Figs. 8*a* and 8*b*). Kraemer et al. (1999) claim that the emission drops by $\sim$20% in the area between the peaks at 20 μm. Our higher resolution images show emission drops by almost 80% at 18 μm and 70% at 10 μm between the peaks, so that the sources appear as separate objects in the mid-infrared. Kraemer et al. (1999) speculate that this source may derive its double-lobed shape because it is a torus or dust disk around a central star. This seems unlikely given that the higher resolution images show elongation in the lobes perpendicular to the plane of the speculated disk.

The near-infrared images of Persi et al. (1996) from this area show that the mid-infrared emission of IRS I3 is coming from a cluster of ($\sim$7) near-infrared sources with extended emission in *H* (Fig. 9) and *K*. The overall extended shape of the near-infrared emission compared to that in the mid-infrared again strengthens our belief that the relative astrometry between the near-infrared and mid-infrared for all these NGC 6334 I sources is accurate. The brightest source coincident with IRS I3 in the *H*-band image of Persi et al. (1996) appears to be located near the central temperature peak (Fig. 9*b*). This bright near-infrared star, which is also seen at *J* and *K*, may be responsible for the central ion-

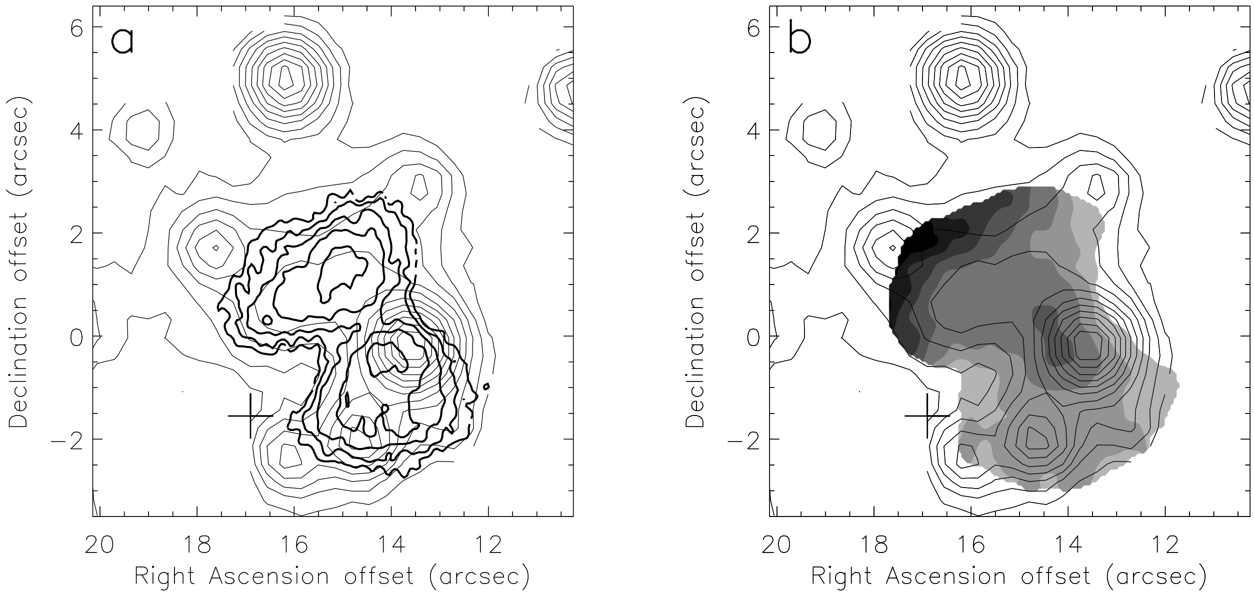

FIG. 9.—Cluster of near-infrared sources coincident with IRS I3; (*a*) shows the *H* band (*thin contours*), overlaid on the Keck 10 μm extended emission (*thick contours*), and (*b*) shows the *H* band overlaid on the color temperature map for IRS I3 (*filled contours*). The low-spatial resolution (~8″) 2.2 μm peak of Becklin & Neugebauer (1974) for IRS I3 is plotted here as a cross. This obvious discrepancy in position has lead us to a revision in the mid-infrared coordinates of IRS I3. The origin in both panels is the same as in Fig. 1.

izing and heating the IRS I3. Another near-infrared source is located just northeast of the northern lobe. This is the location of the temperature maximum in the color temperature maps, and therefore this star may be externally heating this part of the mid-infrared source.

Overlaying the 20 μm image from Harvey & Gatley (1983) with our 18 μm image does show good coincidence between the peaks of IRS I1 and IRS I3. However, the coordinates quoted for this source from Harvey & Gatley (1983) are actually from the 2.2 μm observations of Becklin & Neugebauer (1974). This position is offset from the position of the mid-infrared source we observe and the near-infrared emission of Persi et al. (1996) (Fig. 9). The most likely reason for this difference in position is that the images of Becklin & Neugebauer (1974) were taken with scans from a near-infrared photometer with an effective beam size of ~8″. The offset between the brightest near-infrared source and the position quoted by Becklin & Neugebauer (1974) is 3″.4 in right ascension and 1″.4 in declination, well within the errors they quote of 5″ for right ascension and 4″ for declination.

Because the morphologies and peaks of IRS I3 are different at 10 and 18 μm, and because of the extremely extended nature of the mid-infrared emission, it is difficult to assign reference coordinates to the source. In Figure 8 we arbitrarily show the 10 μm peak in the southern lobe of IRS I3 as the reference position. Coordinates for this position are given in Table 1.

5. CONCLUSIONS

High-resolution mid-infrared observations of the central region of NGC 6334 I have revealed much about the nature and properties of the sources there. The UCHII region NGC 6334F is composed of two sources, IRS I1 and G351.42+0.64:DPT00 2. The peak of IRS I1 appears to be coincident with the peak in the radio continuum. Ammonia observations of Kraemer et al. (1999), when registered properly with our mid-infrared data, indicate that the shape of the UCHII region is not due to a bow shock but instead to champagne-like flow from stellar source at the edge of a molecular clump. Maser emission is concentrated at this interface between the mid-infrared and ammonia emission and may therefore be shock-induced. There are two other strings of masers that lie near the two peaks in the ammonia emission and may be delineating the sites of hot molecular cores that are too young and/or embedded to be seen yet in the mid-infrared.

The mid-infrared emission from IRS I1 seems to be coming from an arc of dust at the interface between the molecular ammonia clump and the UCHII region and may be material swept up by the expanding shock front of the UCHII region. The color temperature peaks at a location interior to this mid-infrared arc, coincident with a near-infrared source IRS 1E. This source may be the stellar source responsible for the ionization and heating of the NGC 6334F region. Two other near-infrared sources, IRS 1W and IRS 1SW, lie in the northern and southern parts of the mid-infrared arc and are associated with the majority of the masers in the region. There is no temperature peak at these locations, so the near-infrared emission may just be reflected or shock excited emission. A fourth near-infrared source (IRS 1SE) seems to simply be reflected emission off the UCHII region tail.

G351.42+0.64:DPT00 2 appears to be a clump of dust, perhaps swept up by the shock front of UCHII region. It displays a steep temperature gradient toward the color temperature peak. It also shows some signs of ionized emission in the higher resolution radio continuum images, but only on the hotter, southern side. For these reasons it may be that DPT00 2 has no central heating source but is simply heated and ionized by the same source heating and ionizing IRS I1 (IRS 1E).

IRS I2 was believed to be associated with the a linear structure of methanol masers and perhaps delineating a circumstellar disk. However, the thermal dust emission is elongated at a different position angle to the position angle of the maser distribution. The low surface brightness, smooth color temperature distribution, and lack of a near-infrared component may indicate that there is no internal stellar source here at all. Furthermore, the masers are offset from the mid-infrared peak and could be associated with the secondary peak in the ammonia distribution.

Lower resolution mid-infrared images of IRS I3 showed it to be a double peaked source. However, the high-resolution images presented here show that it has a complex and peculiar morphology. We find, using the near-infrared data of Persi et al. (1996), that the large and extended mid-infrared sources are extended dust emission from a cluster of stellar sources seen in the near-infrared. These stellar sources have directly influenced the morphology in the mid-infrared and the structure of the source as seen in the color temperature map.

The reality of the 7 mm source in this region has been seriously called into question by the nondetection in the mid-infrared and has recently been discovered to be an artifact of data reduction by follow-up observations of the original authors.

The authors would like to thank NASA's Florida Space Grant Consortium for their financial support of the first author at the time of observations. Data presented herein were obtained at the W. M. Keck Observatory, which is operated as a scientific partnership among the California Institute of Technology, the University of California and the National Aeronautics and Space Administration. The Observatory was made possible by the generous financial support of the W. M. Keck Foundation. The authors wish to recognize and acknowledge the very significant cultural role and reverence that the summit of Mauna Kea has always had within the indigenous Hawaiian community. We are most fortunate to have the opportunity to conduct observations from this mountain.

REFERENCES

Becklin, E. E., & Neugebauer, G. 1974, in ESRO Symp. 105, H II Regions and the Galactic Center, ed. A. F. M. Moorwood (Noordwijk: ESRO), 39
Bloomer, J. D., et al. 1998, ApJ, 506, 727
Carral, P., Kurtz, S. E., Rodriguez, L. F., De Pree, C., & Hofner, P. 1997, ApJ, 486, L103
Carral, P. Kurtz, S. E., Rodriguez, L. F., Menten, K., Canto, J., & Arceo, R. 2002, AJ, 123, 2574
Caswell, J. L. 1997, MNRAS, 289, 203
Cesaroni, R., Churchwell, E., Hofner, P., Walmsley, C. M., & Kurtz, S. 1994, A&A, 288, 903
Claussen, M., Marvel, K. B., Wootten, H. A., & Wilking, B. A. 1997, in IAU Symp. 182, Herbib-Haro Flows and the Birth of Low-Mass Stars, ed. B. Reipurth & C. Bertout (Dordrecht: Kluwer), 515
De Buizer, J. M. 2000, Ph.D. thesis, Univ. Florida
———. 2002, in IAU Symp. 206, Cosmic Masers: From Protostars to Blackholes, ed. V. Migenes (San Francisco: ASP), 18
De Buizer, J. M., Piña, R. K., & Telesco, C. M. 2000, ApJS, 130, 437
De Pree, C. G., Rodgriguez, L. F., Dickel, H. R., & Goss, W. M. 1995, ApJ, 447, 220
Doyon, R. 1990, Ph.D. thesis, Univ. London
Ellingsen, S. P., Norris, R. P., & McCulloch, P. M. 1996, MNRAS, 279, 101
Ellingsen, S. P., et al. 1996, in Proc. 4th Asia-Pacific Telescope Workshop, ed. E. A. King (Sydney: ATNF/CSIRO), 106
Emerson, J. P., Jennings, R. E., & Moorwood, A. F. M. 1973, ApJ, 184, 401
Forster, J. R., & Caswell, J. L. 1989, A&A, 213, 339
Gaume, R. A., & Mutel, R. L. 1987, ApJS, 65, 193
Greenhouse, M. A., Woodward, C. E., Thronson, H. A., Rudy, R. J., Rossano, G. S., Erwin, P., & Puetter, R. C. 1991, ApJ, 383, 164
Harvey, P. M., & Gatley, I. 1983, ApJ, 269, 613
Hofner, P., & Churchwell, E. 1996, A&AS, 120, 283
Kraemer, K. E., Deutsch, L. K., Jackson, J. M., Hora, J. L., Fazio, G. G., Hoffmann, W. F., & Dayal, A. 1999, ApJ, 516, 817
Kraemer, K. E., & Jackson, J. M. 1995, ApJ, 439, L9
Kurucz, R. L. 1979, ApJS, 40, 1
Mathis, J. S. 1990, ARA&A, 28, 37
McBreen, B., Fazio, G. G., Stier, M., & Wright, E. L. 1979, ApJ, 232, L183
McKee, C. F., Chernoff, D. F., & Hollenbach, D. J. 1984, in the 16th ESLAB Symp., Galactic and Extragalactic Infrared Spectroscopy, ed. M. F. Kessler & J. P. Phillips (Dordrecht: Reidel), 103
Neckel, T. 1978, A&A, 69, 51
Persi, P., Roth, M., Tapia, M., Marenzi, A. R., Felli, M., Testi, L., & Ferrari-Toniolo, M. 1996, A&A, 307, 591
Persi, P., Tapia, M., Felli, M., Lagage, P. O., & Ferrari-Toniolo, M. 1998, A&A, 336, 1024
Rodríguez, L. F., Cantó, J., & Moran, J. M. 1982, ApJ, 255, 103
Tapia, M., Persi, P., & Roth, M. 1996, A&A, 316, 102